# Substorm Activity as a Driver of Energetic Pulsating Aurora

Riley Troyer[1], ALLISON JAYNES[1], Stephen Kaeppler[2], Roger Varney[3], Ashton Reimer[3], and Sarah Jones[4]

[1]University of Iowa
[2]Clemson University
[3]Formerly of SRI International
[4]Formerly of NASA Goddard

November 30, 2022

**Abstract**

Pulsating aurora are common diffuse-like aurora that appear as widely varying patches that blink on and off with periods up to 20 seconds. Rocket and incoherent scatter radar studies have suggested that energies of the responsible electrons are higher than other auroral types. However, there has yet to be a statistical study concerning the quantitative energy content of pulsating aurora. In this work, we analyzed the energy spectrum from 55 events. We obtained this by inverting the electron density profile as measured by the Poker Flat Incoherent Scatter Radar. We compared this to magnetic local time (MLT), AE index, and temporal proximity to substorm onset. There was a small propensity for higher energy fluxes between 2 and 4 MLT, but a stronger trend in relation to both temporal substorm proximity and AE index. We found that with rising AE, the average energy flux increased from 0.56 mW/mˆ2 for AE <= 200 to 2.24 mW/mˆ2 for an AE index > 600. Associated, is a spectral hardening where >= 30 keV electrons contribute 13% and 55% respectively. There was also an increase in total energy flux associated with closer temporal proximity to a substorm, although the higher energies remained present for approximately an hour. Our results confirm the high energy nature of pulsating aurora, demonstrate the connection to substorms, and imply their importance to coupling between the magnetosphere and atmosphere.

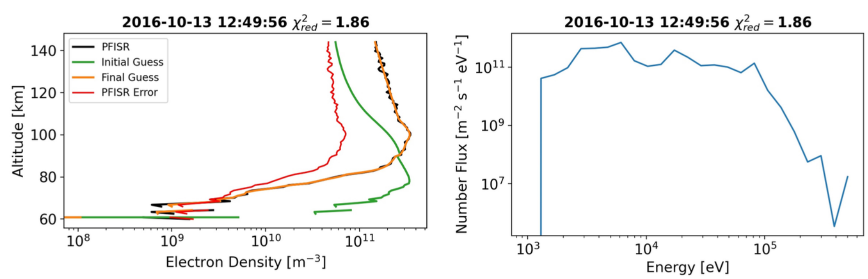

# Substorm Activity as a Driver of Energetic Pulsating Aurora

**R. N. Troyer [1], A. N. Jaynes [1], S. L. Jones [2], S. R. Kaeppler [3], R. H. Varney [4], A. S. Reimer [4]**

[1]Department of Physics and Astronomy, University of Iowa
[2]Formerly of NASA Goddard Space Flight Center
[3]Clemson University
[4]SRI International

**Key Points:**

- We analyzed the inverted energies for 55 pulsating aurora events and found a close relationship to substorms and AE index.
- The average total energy flux and spectral hardness increase closer to substorm onset and for higher AE indices.
- The spectral hardness remains enhanced for approximately 1 hour after substorm onset.

Corresponding author: Riley Troyer, `riley-troyer@uiowa.edu`

## Abstract

Pulsating aurora are common diffuse-like aurora that appear as widely varying patches that blink on and off with periods up to 20 seconds. Rocket and incoherent scatter radar studies have suggested that energies of the responsible electrons are higher than other auroral types. However, there has yet to be a statistical study concerning the quantitative energy content of pulsating aurora. In this work, we analyzed the energy spectrum from 55 events. We obtained this by inverting the electron density profile as measured by the Poker Flat Incoherent Scatter Radar. We compared this to magnetic local time (MLT), AE index, and temporal proximity to substorm onset. There was a small propensity for higher energy fluxes between 2 and 4 MLT, but a stronger trend in relation to both temporal substorm proximity and AE index. We found that with rising AE, the average energy flux increased from $0.56\,\mathrm{mW\cdot m^{-2}}$ for AE $\leq 200$ to $2.24\,\mathrm{mW\cdot m^{-2}}$ for an AE index $> 600$. Associated, is a spectral hardening where $\geq 30\,\mathrm{keV}$ electrons contribute 13% and 55% respectively. There was also an increase in total energy flux associated with closer temporal proximity to a substorm, although the higher energies remained present for approximately an hour. Our results confirm the high energy nature of pulsating aurora, demonstrate the connection to substorms, and imply their importance to coupling between the magnetosphere and atmosphere.



## Plain Language Summary

Not all aurora (northern lights) are bright and defined curtains of light. Diffuse aurora are more modest. Barely visible to the naked eye, they spread across large portions of the night sky and can be easily overlooked. Pulsating aurora are a common and more playful type of diffuse aurora. In one of these displays, widely varying patches of aurora blink on and off with with periods ranging up to 20 seconds. While they aren't as bright, it has been suspected that the electrons which cause pulsating aurora are much more energetic than other types of aurora. Since energetic electrons move faster and thus can reach further into the atmosphere, it is possible that pulsating aurora may affect terrestrial climate. To study this, we first need a better understanding of pulsating aurora energies and how they can vary. In this study, we looked at the energy of 55 pulsating aurora events. In doing so, we confirmed that the energy of pulsating aurora is much higher than other types of aurora. We also found that the most energetic aurora happen close

in time to a magnetic disturbance known as a substorm and that a stronger disturbance leads to higher energies.

## 1 Introduction

Pulsating aurora are a stark contrast to the bright curtains of discrete aurora that often precede them. Diffuse and barely visible to the naked eye, this type of aurora is most often observed a few hours after magnetic midnight (e.g., Oguti et al., 1981; Jones et al., 2011). Often staying out for hours, pulsating aurora can cover large portions of the sky and in some cases expand over entire sections of the auroral region (Jones et al., 2013). Using SuperDarn and imager data, E. Bland et al. (2021) found that around half of pulsating aurora events extend between 4-5 hours of magnetic local time and between 62° to 70° in magnetic latitude. Over this area, auroral patches blink on and off with periods ranging up to around 20 seconds (e.g., Davis, 1978; Lessard, 2012). Adding to the show, individual patches can be remarkably varied with differing periods, shapes, and sizes typically between 10s to 100s of kilometers (Johnstone, 1978; Lessard, 2012). See Figure 1 panels A1-A3 as an example.

Some studies have attempted to classify different types of pulsating aurora. For instance, Royrvik and Davis (1977) classified events into patches, arcs, and arc segments. More recently, Grono and Donovan (2018) made a distinction between the quickly varying amorphous pulsating aurora, more regular patchy pulsating aurora, and non-pulsating patchy aurora. We included all of these when making a general identification of pulsating aurora.

Numerous studies have shown that the electrons responsible for pulsating aurora originate in the equatorial region of the outer Van Allen radiation belt. These electrons are pitch-angle scattered into the upper-atmosphere through wave-particle interactions, most likely with lower-band chorus waves (Nishimura et al., 2010, 2011; Jaynes et al., 2013; Kasahara et al., 2018; Hosokawa et al., 2020). Previous studies have found that the energy of these particles is substantially higher than other auroral types, ranging between 10s to 100s of keV (e.g., Whalen et al., 1971; Sandahl et al., 1980). This energy can vary substantially, even within individual events. Jones et al. (2009) notes often seeing a decrease in energy throughout an event. Hosokawa and Ogawa (2015) found, using the European Incoherent Scatter Radar, that the energy spectrum of pulsating aurora is harder when a patch is "on" versus when it is "off" with only background aurora present.

Several papers concerning the height of pulsating aurora indicate that there may also be some relation between energy and substorm onset. In the two events that they analyzed, Oyama et al. (2017) found that the atmospheric electron densities associated with pulsating aurora dropped to a lower altitude following a substorm. This would indicate an influx of higher energy electrons capable of penetrating further into the atmosphere. These results match up with the statistical study of Hosokawa and Ogawa (2015) who showed that the electron density profile of pulsating aurora extends lower in altitude during periods with a large AE index ($> 500$). This previous work is a strong indicator of the increase in higher energy electrons, or spectral hardening, during geomagnetically perturbed conditions. However, the results are qualitative as altitude is only a proxy for energy. Wing et al. (2013) did conduct a statistical study of auroral energies associated with substorm onset. They made distinctions between broadband (Alfvén accelerated) electrons, monoenergetic (parallel electric field accelerated) electrons, and diffuse (whistler mode wave scattered) electrons. They found that energies increase in association to substorms for all types, with the largest for diffuse electrons. However, they made no distinction between general diffuse and pulsating aurora. Thus, there is a need for a statistical study concerning the energy of pulsating aurora and how it can predictably vary with magnetospheric driving.

## 2 Data

This paper presents a data set of 57 pulsating aurora events (due to missing model indices we couldn't invert two of these) captured over 51 days with the Poker Flat Research Range All Sky Imager (PFRR ASI). A table of these days can be found in the supplemental material. This instrument takes an image approximately every 12 seconds at 428 nm, 557 nm, and 630 nm. We used the 428 nm images because they corresponds to a lower altitude that the higher energy electrons of pulsating aurora more often reach to. It is worth noting that despite the 12 second period of the camera, we can still accurately identify pulsating aurora, see Figure 1 panels A1-A3.

For each of these pulsating aurora events, the Poker Flat Incoherent Scatter Radar (PFISR) ran a MSWinds experiment (Kaeppler et al., 2020). This mode is tuned for the

D-region of the atmosphere and provides electron density as a function of altitude and time. The spatial scale of the measurements range between 40 and 144 km with a 0.75 km resolution. Temporally, the data is integrated over one minute (Janches et al., 2009). The MSWinds experiment measures in four beam directions. We used the vertical beam as it has the best statistics and is a negligible angle away from the parallel magnetic field direction ($< 20°$). Figure 1 panel B is an example of electron densities measured by PFISR MSWinds23 during a period of typical pulsating aurora on October 13, 2016. This event began just after a substorm and continued until the end of the PFISR experiment. This data is also an excellent example of the electron density profile pushing to lower altitudes during pulsating aurora. For additional PFISR information see Appendix B.

## 3 Analysis

In this study, we attempt to quantify the energy spectra of pulsating aurora, in particular, the higher energy portion of the spectrum. Much of the previous work has indicated that the energy of pulsating aurora varies significantly both within and between events (Jones et al., 2009; Wing et al., 2013; Hosokawa & Ogawa, 2015). Based on these results, we chose to examine variations related to magnetic local time (MLT), AE index, and an epoch associated with temporal substorm proximity. We set an epoch time of 0 to substorm onsets taken from lists created by Newell and Gjerloev (2011), Forsyth et al. (2015), and Ohtani and Gjerloev (2020). We chose these three lists because they cover a time period that encompasses our data. Each method identifies substorms in a slightly different way, so by including all three we can identify more events over a broader range of criteria. We limited these substorms to those that occurred within $\pm 15°$ longitude and $\pm 8°$ latitude of the Poker Flat Research Range. For the AE indices, we used archived 10-minute predicted values (Luo et al., 2013).

As a proxy for energy, we chose the lower altitude boundary that PFISR measured a number density of $N_e = 10^{10}\,\mathrm{m}^{-3}$ for each 1-minute integrated altitude profile. Additionally, to meet this criteria, the associated error had to be less than $5 \times 10^{9}\,\mathrm{m}^{-3}$. We chose these values somewhat arbitrarily given that it is a round number near the detection limit of PFISR. However, we did test the sensitivity and found them to be acceptably insensitive. We then plotted the lower boundaries against MLT, substorm proximity, and AE index.

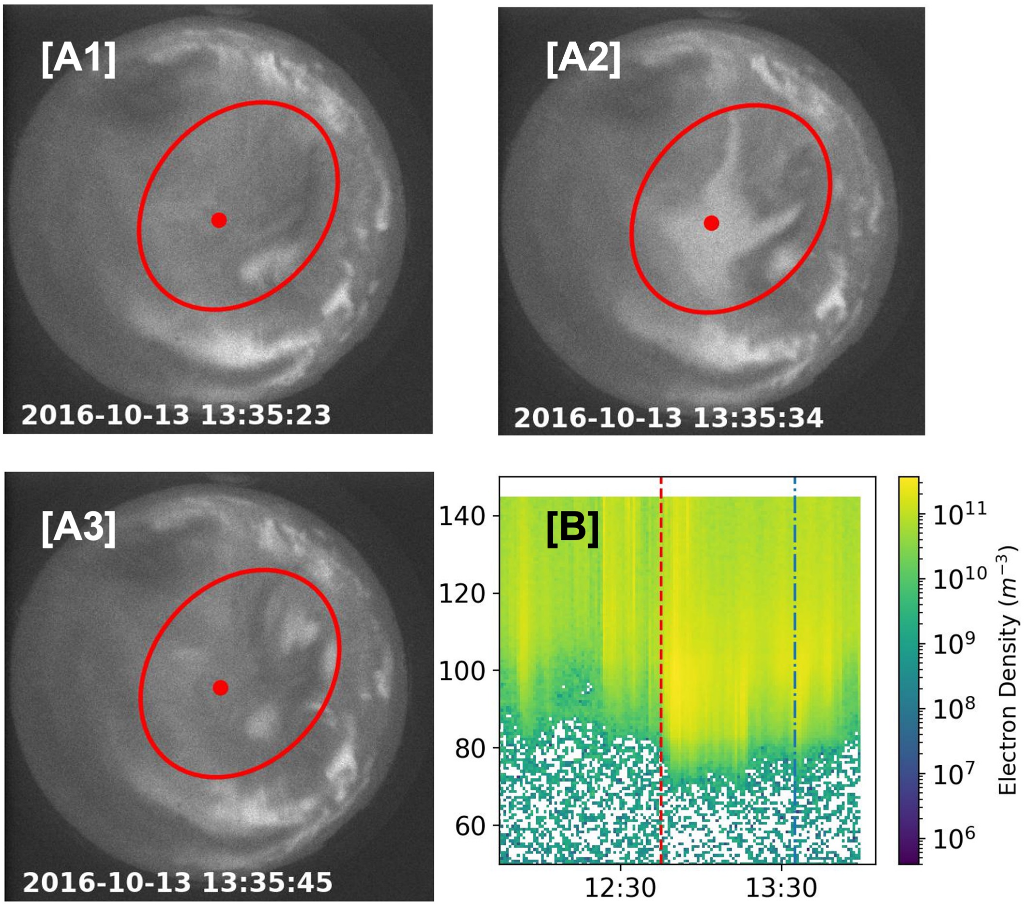


**Figure 1.** Panels A1-A3 show a series of 428 nm images from the Poker Flat Research Range All Sky Imager with several pulsating aurora patches of differing sizes. Even though the imaging rate is 12 seconds, we can still identify pulsating aurora. The red dot indicates the center of each image and thus the approximate location of the vertical PFISR beam. Panel B is the PFISR electron number density data for a pulsating aurora event on October 13, 2016. The data is plotted vs. altitude in km and universal time. The dashed red line indicates the start of pulsating aurora. The dashed and dotted blue line indicates when the images were taken. The radar stopped taking data before the pulsating aurora ended.

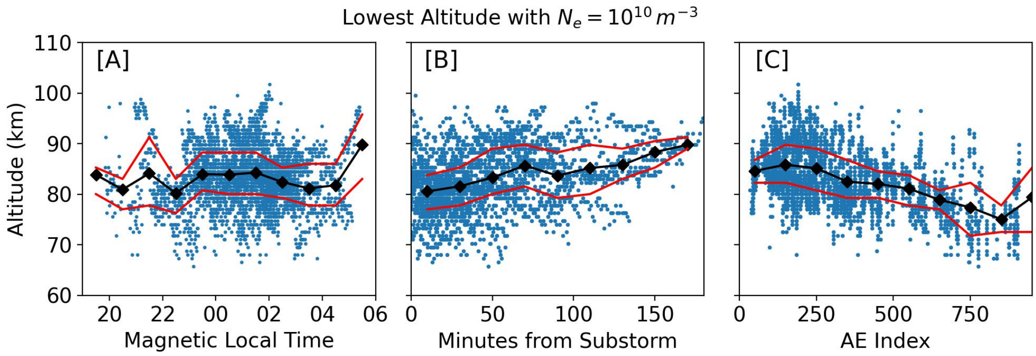


**Figure 2.** Lowest altitude PFISR measurements during pulsating aurora with $N_e = 10^{10}\,\mathrm{m}^{-3}$ plotted versus magnetic local time [A], time from the nearest substorm onset [B], and AE index [C]. The black diamonds indicate the average altitude for the surrounding hour, 20 minutes, 200 AE units respectively. The red lines indicate the 25% and 75% quartiles.

### 3.1 Magnetic Local Time

Figure 2 panel A shows the altitude boundary values compared to MLT as calculated from the IGRF model for 2020. As we would expect, a majority of the measurements occurred several hours after magnetic midnight. Previous studies have shown that this is the most common time for pulsating aurora (Oguti et al., 1981; Jones et al., 2011). However, our data is biased towards common pulsating aurora times, as this is when we requested runs. The hourly averages shown by the black diamonds centered on each hour indicate that there may be a dip between 2 to 4 MLT, similar to previous results (Hosokawa & Ogawa, 2015; Partamies et al., 2017; E. C. Bland et al., 2019; Nanjo et al., 2021). However, due to the wide scatter of data and limited statistics for several time bins, it's difficult to say how significant this behavior is in our data.

### 3.2 Substorm Proximity and AE index

Figure 2 panel B shows the altitude boundary values compared to temporal substorm proximity. Here we see that lower altitudes are more common closer to the start of a substorm, indicating a hardening of the spectrum.

Figures 2B and 2C shows the altitude boundary values compared to AE index. Similar to substorm proximity, there is a clear relation between a higher AE value and lower altitudes. This matches well with Hosokawa and Ogawa (2015) who found that the peak

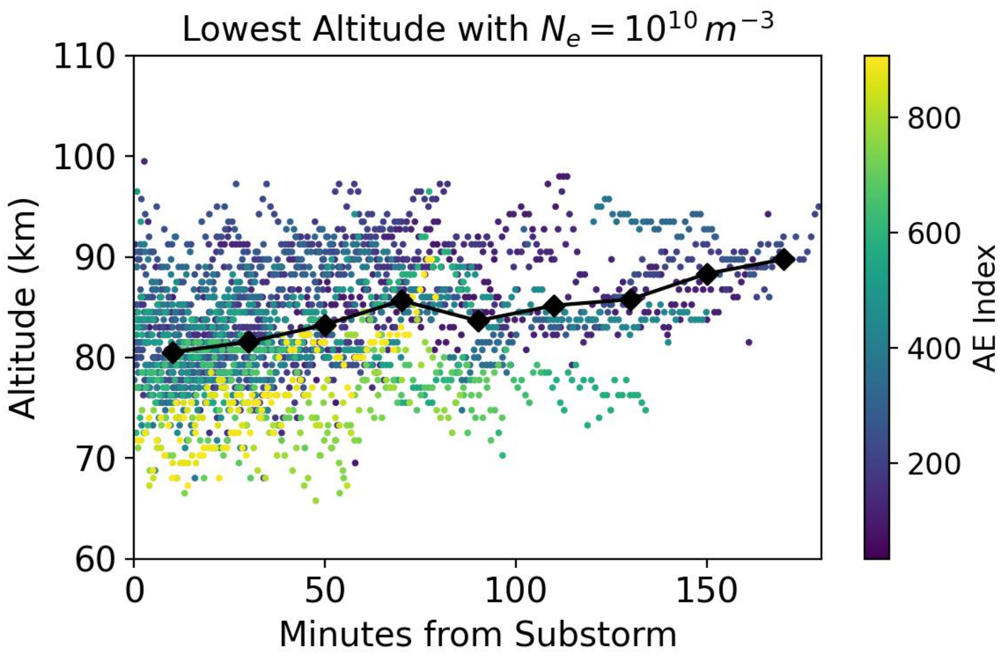


**Figure 3.** Lowest altitude PFISR measurements during pulsating aurora with $N_e = 10^{10}\,\mathrm{m}^{-3}$ plotted versus time from the nearest substorm onset. The markers are colored based on AE index. The black diamonds indicate the average altitude for the surrounding 20 minutes.

height of pulsating aurora lowers during higher AE indices. However, our data may be more representative of the higher energy side of the spectrum since we used a lower boundary value.

We combined Figures 2B and 2C to produce Figure 3. Here we have colored the markers of Figure 2 panel B based on AE index. This result shows that both temporal substorm proximity and AE index play a role in varying the lower altitude boundary. The lowest altitudes tend to occur with both a high AE index and close temporal proximity to a substorm.

### 3.3 Energy Spectra from Electron Density Inversion

Our analysis of the lower altitude boundary with $N_e = 10^{10}\,\mathrm{m}^{-3}$ indicates that both AE index and temporal substorm proximity have significant impacts on how hard the pulsating aurora energy spectrum can be. However, this metric is only a proxy for energy. To investigate further, we solved the inverted problem required to convert the PFISR electron densities into energy spectra. To do this, we used the process outlined in Semeter and Kamalabadi (2005). In doing so, we assumed that the pitch angle distribution was isotropic (Whalen et al., 1971; Sandahl et al., 1980), and that the electron density varies slowly compared to our time scales. We describe our exact implementation of the inversion process in Appendix A. We also included an example fitted electron density and the associated energy spectrum as a supplemental figure. In an analysis like this, there are multiple spectra that could result in a reasonably good fit of the density profile, making the problem ill-defined. To help mitigate this, we chose the solution that maximized the Berg Entropy. As Semeter and Kamalabadi (2005) states, this solution "may be viewed as the most noncommittal approach with respect to the unavailable information." To further reduce uncertainty, we chose an energy threshold of 30 keV to separate the low and high portions of the energy spectrum and integrated the two regions. This gives us an average low and high energy flux and limits the dependency of our results on the spectral shape.

The largest source of error in the inversion process is likely the assumed atmospheric chemistry that connects PFISR observations to an ionization rate. This is not well known, especially for the D-region. As our primary chemistry model we used the Glukhov-Pasko-Ina (GPI) model (Glukhov et al., 1992; Lehtinen & Inan, 2007). This has been shown to perform well for the D-region (Marshall et al., 2019). However, it is not well defined in the E-region. To account for this, we set the values above 90 km to those calculated by Gledhill (1986) for nighttime aurora. The Gledhill model is suitably close that of Vickrey et al. (1982) above 90 km and the Vickrey model has been shown to perform well in this region (Sivadas et al., 2017). While we could have used the Vickrey model, we believe the Gledhill model is slightly better for this data. However, both models are only rough estimates. We refer to this adjusted model as GPI+. To provide context to our results calculated using GPI+, we inverted each density profile using three additional chemistry models. These results can be found in Appendix A.

After performing the inversions, we found the geometric mean for $\geq 30$ keV and $< 30$ keV electrons in bins relative to substorm onset and AE index. Figure 4 shows the results. While not shown here, we found similar relative behavior in analyses for energy thresholds of 50 keV and 100 keV. For $< 20$ min the high energy contributions were 13% and 1.3% respectively. For $> 600$ AE these were 35% and 2.6% respectively.

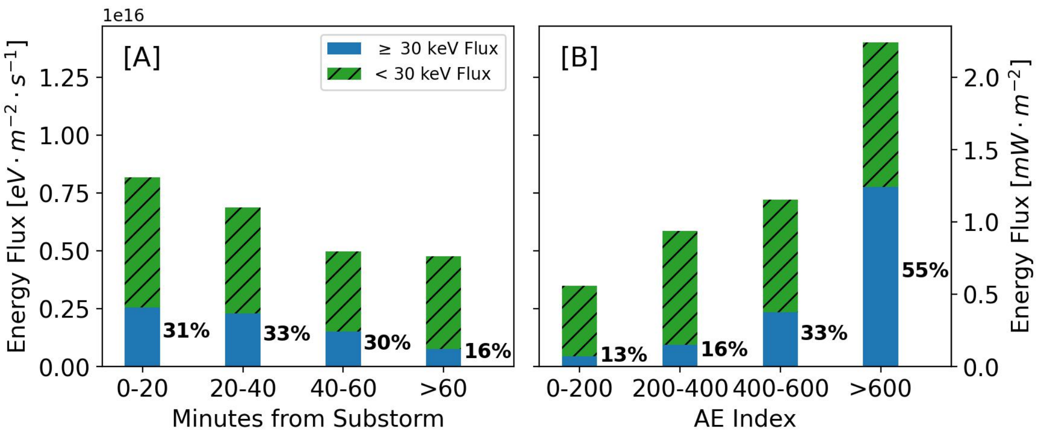


**Figure 4.** The high ($\geq$ 30 keV) and low ($<$ 30 keV) energy flux contributions to pulsating aurora events occurring in four temporal bins relative to substorm onset [A] and AE index [B].

## 4 Discussion

Before discussing our results, it is worth mentioning possible sources of systematic error. One, several previous studies found that the electron density and energy spectra shifts towards higher energies during the on phase of pulsating aurora (Hosokawa & Ogawa, 2015; Whalen et al., 1971). Our data is integrated over one minute, so these variations will likely be smoothed out, thus reducing the spectral hardness. Two, we are not capturing the full spectrum of electron precipitation. Ionization associated with electron energies less than about 1 keV, peaks above the altitudes that PFISR measures in the D-region mode (Fang et al., 2010). If the energy flux for this portion of the spectrum is significant, we could be overestimating the spectral hardness and underestimating the total energy. Three, the instrument sensitivity limits our ability to detect higher energy particles with lower fluxes. If populations such as these are present, we could be underestimating the spectral hardness. Four, we only selected pulsating aurora that were in the center of the imager, but we didn't account for times that the PFISR beam wasn't directly on a pulsating patch. If the precipitating flux is highly local, we could be underestimating the energy flux during such periods.

Figure 4 shows how the energy composition of pulsating aurora varies with respect to both substorm proximity [A] and AE index [B]. Within an hour of a substorm around a third of the total energy flux is carried by $\geq$ 30 keV electrons. At $>$ 60 minutes this drops to around a sixth. Interestingly, while the total energy flux climbs closer to the substorm, the energy composition remains similar all the way out to an hour after onset. This indicates that the initial substorm "kick" hardens the spectrum and it remains hard up to an hour afterwards, even as the total energy flux decreases.

The energy spectrum associated with AE index varies even more dramatically. In highly perturbed times of AE $> 600$ over a half of the average energy flux is carried by the $\geq 30$ keV electrons. This again drops to just over a tenth for quiet periods of AE $\leq 200$. Assumptions about the atmospheric chemistry can vary these values, but for every model we found the same relative behavior. The relative behavior was also the same when we used threshold values of 50 keV and 100 keV. Thus, we speculate with a high level of confidence that pulsating auroral energies are varied by both the strength of a substorm as well as temporal proximity to it.

Combining our results with those of E. Bland et al. (2021), we can perform a back-of-the-envelope calculation to estimate the incoming power of a typical pulsating aurora event. We will assume an event extending between 62° and 70° magnetic latitude and 4 hours of magnetic local time. Using this, approximately 5.4 gigawatts (GW) of power would be entering the atmosphere during periods with AE $> 600$ with 2.7 GW coming from $\geq$ 30 keV electrons. For periods $<$ 20 minutes after substorm onset and all AE indices these values are 2.9 GW and 0.9 GW respectively.

Our results are significant as they indicate a process connecting substorms and pulsating aurora. There is a well documented relation between substorm activity post-midnight and whistler-mode wave generation near the equator (Tsurutani & Smith, 1974; Thorne et al., 1974). The proposed mechanism connecting them is Doppler-shifted cyclotron resonance with 10-100 keV substorm injected electrons (Dungey, 1963; Kennel & Petschek, 1966). In addition, the amplitude of already present whistler-mode waves can vary with substorm injection. Meredith et al. (2000) showed that between $3.8 < L < 6$ whistler-mode amplitudes increased after a substorm and then decayed with a timescale of $\tau \approx$ 1.1 hours. That value is similar to the timescale over which we see a decrease in the spectral hardness. Given that whistler-mode waves are known to drive pulsating aurora, this is one likely explanation. Additionally, the MLT dependence of substorm driven whistler-mode waves could explain the slight increase in energetic pulsating aurora events we see post-midnight (Tsurutani & Smith, 1977).

Our results also confirm, as previous studies have hinted at, that the energetic nature of pulsating aurora is inherent to the phenomenon and not just a result of a few extreme events. This is important because pulsating aurora are very common (Oguti et al., 1981) and can be long-lasting (Jones et al., 2013). Thus they represent a relatively large transfer of energy between the magnetosphere and lower ionosphere. When considering the effects of this transfer, the total energy flux is clearly important, but so too is the hardness of the energy spectrum. Higher energy electrons reach further into the atmosphere and thus have a higher probability of influencing terrestrial climate through processes like $NO_x$ based ozone depletion (Turunen et al., 2016; Verronen et al., 2021, & and references therein). We found that the hardest spectra occur close in time to a substorm and for high AE indices. In short, our results can be used to more accurately parameterize the atmospheric consequences of pulsating aurora.

## 5 Summary

- The energy flux of pulsating aurora correlates strong with the temporal substorm proximity and AE index.
- In relation to temporal substorm proximity the total energy flux varies between 1.31 and $0.76\,\mathrm{mW} \cdot \mathrm{m}^{-2}$ for $\leq 20$ and $> 60$ minutes. The associated contribution to the total energy flux from $\geq 30$ keV electrons are 31% and 16%.
- In relation to substorms, the energy spectrum remains hard out to 1 hour after onset before softening.
- In relation to AE index the total energy flux varies between 2.24 and $0.56\,\mathrm{mW} \cdot \mathrm{m}^{-2}$ for $> 600$ and $\leq 200$ AE indices. The associated contributions to the total energy flux from $\geq 30$ keV electrons are 55% and 13%.
- We estimate that for a typically pulsating auroral event occurring $< 20$ min after substorm onset (AE $> 600$), approximately 2.9 (5.4) GW of power enters the atmosphere. The contributions from $\geq 30$ keV electrons are 0.9 (2.7) GW.

## Appendix A Inversion Technique

To solve the inverted problem of extracting an energy spectrum from electron densities, we used the process outlined in Semeter and Kamalabadi (2005). We assumed the pitch angle distribution of the incoming electrons was isotropic and used the universal energy dissipation function ($\Lambda$) given in the paper. We took our range-energy function from Barrett and Hays (1976) as

$$R = 4.7 \times 10^{-6} + 5.36 \times 10^{-5} K^{1.67} - 0.38 \times 10^{-7} K^{-0.7} \qquad [\mathrm{kg} \cdot \mathrm{m}^{-2}]$$

where $K$ is the electron energy in keV. Using these, we can construct a matrix $A$, where

$$A_{ij} = \frac{\Lambda\left(\frac{s(z_i)}{R(K_j)}\right) \rho(z_i) K_j \Delta K_j}{35.5 R(K_j)}$$

where $s(z_i) = \sec(\theta) \int_{z_0}^{\infty} \rho(z)\, dz$ is the mass distance traveled by an electron as a function of altitude. We assumed the dip angle of the magnetic field, $\theta \approx 0$. We calculated the neutral atmospheric density $\rho(z)$ using the NRLMSISE00 model and approximated $z \to \infty$ as $z = 1000$ km (Hedin, 1991).

The matrix $A$ relates the ion production rate ($q$) and the differential number flux ($\phi$) via

$$q_i = A_{ij} \frac{\phi_j}{\Delta K_j}$$

As Fang et al. (2010) showed, using a range-energy function gives poor estimates of the ion production rate from electrons below 1 keV. However, the altitude range of the PFISR data means that there is very little, if any, contribution from these energies. Therefore, we assume that the range-energy function is a good enough estimate in this case.

Important atmospheric chemistry is encapsulated in the conversion of electron density measured by PFISR to an ion production rate. This is especially relevant below 85 km, where the chemistry of ion production becomes increasingly complex (Mitra, 1981). There are several ways of handling the chemistry. The simplest models describe this relation with the continuity equation

$$\frac{dn}{dt} = q - \alpha n^2$$

Assuming the temporal change of the electron density, as measured by PFISR, is small compared to the timescales we are studying, we can say that $q = \alpha n^2$, where $\alpha$ is the effective recombination coefficient. From our experience, this steady state assumption is good for pulsating aurora, at least when integrated over 1 minute like the PFISR data is.

In a model that uses this description, the chemistry is encapsulated in the coefficient. However, obtaining an accurate estimate of $\alpha$ is difficult in practice. For our primary results we used the Glukhov-Pasko-Ina (GPI) model (Glukhov et al., 1992; Lehtinen & Inan, 2007). This uses the specific conditions as measured by PFISR, and modeled by the International Reference Ionosphere (IRI-2016) and NRLMSISE-00. Previous work has shown that GPI performs well for the D-region (Marshall et al., 2019). However, it is not well defined in the E-region. To account for this, we set the values above 90 km to those of Gledhill (1986) for nighttime aurora. The Gledhill model is suitably close that of Vickrey et al. (1982) above 90 km and the Vickrey model performs well in this region (Sivadas et al., 2017). While we could have used the Vickrey model, we believe the Gledhill model is slightly more accurate to this data. We refer to this adjusted model as GPI+. Given that the the chemistry in this region of the atmosphere is not well known, we also performed our analysis with three additional models to provide context.

1. The best fit from Vickrey et al. (1982) of multiple observations from several authors of $\alpha$ in the E-region.

   $$\alpha(h) = 2.5 \times 10^{-12} e^{-h_{\mathrm{km}}/51.2} \qquad [\mathrm{m}^3 \cdot \mathrm{s}^{-1}]$$

   To use this model we needed to extend it into the D-region, where it is not well defined.

2. The observations of Osepian et al. (2009) during a solar proton event on January 17, 2005 at 9:50 UT. While these observations cover the D-region, they must be extended into the E-region. They also only cover a single event and that event is not pulsating aurora.

3. The best fit of Gledhill (1986) for nighttime aurora covering the E-region and D-region.

   $$\alpha(h) = 4.3 \times 10^{-6} e^{-2.42\times10^{-2} h_{\mathrm{km}}} + 8.16 \times 10^{12} e^{-0.524 h_{\mathrm{km}}} \qquad [\mathrm{cm}^3 \cdot \mathrm{s}^{-1}]$$

Figure A1 shows how these three additional chemistry model compare with our analysis. They are represented by scatter points around each bar. These points can be considered as rough bounds on our results.

To determine the differential number flux ($\phi$) we iterated using the maximum entropy method outlined in Semeter and Kamalabadi (2005). We monitored convergence through the $\chi^2$ value between the modeled ion production rate and the rate calculated from the PFISR measurements. We stopped iterating when the step difference in the $\chi^2$

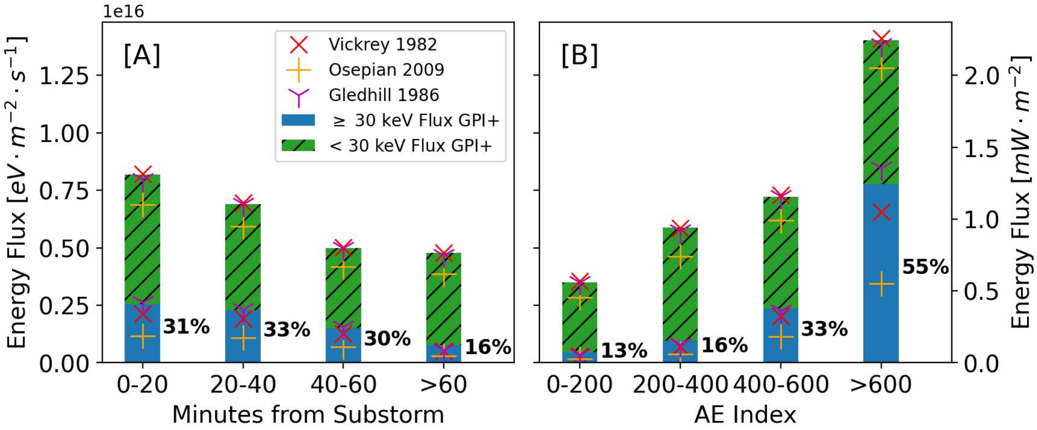


**Figure A1.** The high ($\geq 30$ keV) and low ($< 30$ keV) energy flux contributions to pulsating aurora events occurring in four temporal bins relative to substorm onset [A] and AE index [B]. We set the bar heights to the GPI+ model. The scatter points indicate the individual values from the three other chemistry models.

values was less than 0.01. This usually took between 100 and 1000 steps. From the spectra that converged, we took those with a $1 \leq \chi^2_{\mathrm{reduced}} < 3$ to be suitably good models. To calculate $\chi^2$ it is important to have an accurate description of the variances (errors) in the PFISR data. The data products contain absolute errors associated with the measured number density. To propagate this to the ion production rate we calculated an intermediary recombination coefficient, $\alpha_{\mathrm{chem}}(z) = q_{\mathrm{chem}}(z)/n(z)^2$. Our errors were then

$$\Delta q_{\mathrm{chem}}(z) = 2\alpha_{\mathrm{chem}}(z)n(z)\Delta n(z)$$

To determine $\chi^2_{\mathrm{reduced}}$ we need an estimate of the degrees of freedom in the model. We set this as the number of altitude bins where the errors were less than the data (fitted values) minus the number of energy bins (varied values).

When performing the inversion, we found that the differential number flux of the highest energy bin was often over an order of magnitude larger than the next highest bin. We believe this is not physical and instead an artifact due to the initial electron density guess only needing to converge to the PFISR sensitivity ($\sim 10^9\ \mathrm{m}^{-3}$) and not zero for lower altitudes. To mitigate this error, we only calculated our averages up to the second highest energy bin.

## Appendix B PFISR Data

For this work, we used PFISR data that was taken during the MSWinds experiments. These experiments use a barker code pulse pattern that allows better sensitivity in the D-region atmosphere. In this mode, the instrument estimates electron density from the received power.

We assumed that any signal below 60 km was unphysical in regards to precipitating electrons and took the average signal between 55 and 60 km as our baseline background. We then subtracted this background from the entire electron density profile. In an ideal world, the background would average to 0, but due to hardware constraints after late 2016, the PFISR system has difficulty properly calibrating this and it can be as high as $1 \times 10^9\,\mathrm{m}^{-3}$. These steps are required so we don't get errant estimates of the high energy portion of the spectrum.

**Acknowledgments**

We acknowledge the help and advice of Dr. Robert Marshall, Dr. Nithin Sivadas, and Dr. Pekka Verronen in developing our inversion analysis.

We acknowledge the substorm timing list identified by the SOPHIE technique (Forsyth et al., 2015), the Newell and Gjerloev technique (Newell & Gjerloev, 2011), the Ohtani and Gjerloev technique (Ohtani & Gjerloev, 2020), the SMU and SML indices (Newell & Gjerloev, 2011); and the SuperMAG collaboration (Gjerloev, 2012).

This work was supported by the NASA FINESST award: 80NSSC20K1514.

## References

Barrett, J. L., & Hays, P. B. (1976, January). Spatial distribution of energy deposited in nitrogen by electrons. *Journal of Chemical Physics*, *64*(2), 743-750. doi: 10.1063/1.432221

Bland, E., Tesema, F., & Partamies, N. (2021, February). D-region impact area of energetic electron precipitation during pulsating aurora. *Annales Geophysicae*, *39*(1), 135-149. doi: 10.5194/angeo-39-135-2021

Bland, E. C., Partamies, N., Heino, E., Yukimatu, A. S., & Miyaoka, H. (2019, July). Energetic Electron Precipitation Occurrence Rates Determined Using the Syowa East SuperDARN Radar. *Journal of Geophysical Research (Space*

*Physics)*, *124* (7), 6253-6265. doi: 10.1029/2018JA026437

Davis, T. N. (1978, January). Observed microstructure of auroral forms. *Journal of Geomagnetism and Geoelectricity*, *30* (4), 371-380. doi: 10.5636/jgg.30.371

Dungey, J. W. (1963, June). Loss of Van Allen electrons due to whistlers. *Planetary and Space Science*, *11* (6), 591-595. doi: 10.1016/0032-0633(63)90166-1

Fang, X., Randall, C. E., Lummerzheim, D., Wang, W., Lu, G., Solomon, S. C., & Frahm, R. A. (2010, November). Parameterization of monoenergetic electron impact ionization. *Geophysical Research Letters*, *37* (22), L22106. doi: 10.1029/2010GL045406

Forsyth, C., Rae, I. J., Coxon, J. C., Freeman, M. P., Jackman, C. M., Gjerloev, J., & Fazakerley, A. N. (2015, December). A new technique for determining Substorm Onsets and Phases from Indices of the Electrojet (SOPHIE). *Journal of Geophysical Research (Space Physics)*, *120* (12), 10,592-10,606. doi: 10.1002/2015JA021343

Gjerloev, J. W. (2012, September). The SuperMAG data processing technique. *Journal of Geophysical Research (Space Physics)*, *117* (A9), A09213. doi: 10.1029/2012JA017683

Gledhill, J. A. (1986, June). The effective recombination coefficient of electrons in the ionosphere between 50 and 150 km. *Radio Science*, *21* (3), 399-408. doi: 10.1029/RS021i003p00399

Glukhov, V. S., Pasko, V. P., & Inan, U. S. (1992, November). Relaxation of transient lower ionospheric disturbances caused by lightning-whistler-induced electron precipitation bursts. *Journal of Geophysical Research*, *97* (A11), 16971-16979. doi: 10.1029/92JA01596

Grono, E., & Donovan, E. (2018, June). Differentiating diffuse auroras based on phenomenology. *Annales Geophysicae*, *36* (3), 891-898. doi: 10.5194/angeo-36-891-2018

Hedin, A. E. (1991, February). Extension of the MSIS thermosphere model into the middle and lower atmosphere. *Journal of Geophysical Research*, *96* (A2), 1159-1172. doi: 10.1029/90JA02125

Hosokawa, K., Miyoshi, Y., Ozaki, M., Oyama, S. I., Ogawa, Y., Kurita, S., . . . Fujii, R. (2020, February). Multiple time-scale beats in aurora: precise orchestration via magnetospheric chorus waves. *Scientific Reports*, *10* , 3380. doi:

10.1038/s41598-020-59642-8

Hosokawa, K., & Ogawa, Y. (2015, July). Ionospheric variation during pulsating aurora. *Journal of Geophysical Research (Space Physics)*, *120*(7), 5943-5957. doi: 10.1002/2015JA021401

Janches, D., Fritts, D. C., Nicolls, M. J., & Heinselman, C. J. (2009, May). Observations of D-region structure and atmospheric tides with PFISR during active aurora. *Journal of Atmospheric and Solar-Terrestrial Physics*, *71*(6-7), 688-696. doi: 10.1016/j.jastp.2008.08.015

Jaynes, A. N., Lessard, M. R., Rodriguez, J. V., Donovan, E., Loto'Aniu, T. M., & Rychert, K. (2013, August). Pulsating auroral electron flux modulations in the equatorial magnetosphere. *Journal of Geophysical Research (Space Physics)*, *118*(8), 4884-4894. doi: 10.1002/jgra.50434

Johnstone, A. D. (1978, July). Pulsating aurora. *Nature*, *274*(5667), 119-126. doi: 10.1038/274119a0

Jones, S. L., Lessard, M. R., Fernandes, P. A., Lummerzheim, D., Semeter, J. L., Heinselman, C. J., ... Asamura, K. (2009, May). PFISR and ROPA observations of pulsating aurora. *Journal of Atmospheric and Solar-Terrestrial Physics*, *71*(6-7), 708-716. doi: 10.1016/j.jastp.2008.10.004

Jones, S. L., Lessard, M. R., Rychert, K., Spanswick, E., & Donovan, E. (2011, March). Large-scale aspects and temporal evolution of pulsating aurora. *Journal of Geophysical Research (Space Physics)*, *116*(A3), A03214. doi: 10.1029/2010JA015840

Jones, S. L., Lessard, M. R., Rychert, K., Spanswick, E., Donovan, E., & Jaynes, A. N. (2013, June). Persistent, widespread pulsating aurora: A case study. *Journal of Geophysical Research (Space Physics)*, *118*(6), 2998-3006. doi: 10.1002/jgra.50301

Kaeppler, S. R., Sanchez, E., Varney, R. H., Irvin, R. J., Marshall, R. A., Bortnik, J., ... Reyes, P. M. (2020). Chapter 6 - incoherent scatter radar observations of 10–100kev precipitation: review and outlook. In A. N. Jaynes & M. E. Usanova (Eds.), *The dynamic loss of earth's radiation belts* (p. 145-197). Elsevier. Retrieved from `https://www.sciencedirect.com/science/article/pii/B9780128133712000068` doi: https://doi.org/10.1016/B978-0-12-813371-2.00006-8

Kasahara, S., Miyoshi, Y., Yokota, S., Mitani, T., Kasahara, Y., Matsuda, S., … Shinohara, I. (2018, February). Pulsating aurora from electron scattering by chorus waves. *Nature*, *554*(7692), 337-340. doi: 10.1038/nature25505

Kennel, C. F., & Petschek, H. E. (1966, January). Limit on Stably Trapped Particle Fluxes. *Journal of Geophysical Research (Space Physics)*, *71*, 1. doi: 10.1029/JZ071i001p00001

Lehtinen, N. G., & Inan, U. S. (2007, April). Possible persistent ionization caused by giant blue jets. *Geophysical Review Letters*, *34*(8), L08804. doi: 10.1029/2006GL029051

Lessard, M. R. (2012). A review of pulsating aurora. In *Auroral phenomenology and magnetospheric processes earth and other planets* (Vol. 197, pp. 5673–68). Washington, D.C. :: American Geophysical Union.

Luo, B., Li, X., Temerin, M., & Liu, S. (2013, December). Prediction of the AU, AL, and AE indices using solar wind parameters. *Journal of Geophysical Research (Space Physics)*, *118*(12), 7683-7694. doi: 10.1002/2013JA019188

Marshall, R. A., Xu, W., Kero, A., Kabirzadeh, R., & Sanchez, E. (2019, February). Atmospheric effects of a relativistic electron beam injected from above: chemistry, electrodynamics, and radio scattering. *Frontiers in Astronomy and Space Sciences*, *6*, 6. doi: 10.3389/fspas.2019.00006

Meredith, N. P., Horne, R. B., Johnstone, A. D., & Anderson, R. R. (2000, June). The temporal evolution of electron distributions and associated wave activity following substorm injections in the inner magnetosphere. *Journal of Geophysical Research*, *105*(A6), 12907-12918. doi: 10.1029/2000JA900010

Mitra, A. P. (1981, August). Chemistry of middle atmospheric ionization - a review. *Journal of Atmospheric and Terrestrial Physics*, *43*, 737-752. doi: 10.1016/0021-9169(81)90050-7

Nanjo, S., Hozumi, Y., Hosokawa, K., Kataoka, R., Miyoshi, Y., Oyama, S.-i., … Kurita, S. (2021, October). Periodicities and Colors of Pulsating Auroras: DSLR Camera Observations From the International Space Station. *Journal of Geophysical Research (Space Physics)*, *126*(10), e29564. doi: 10.1029/2021JA029564

Newell, P. T., & Gjerloev, J. W. (2011, December). Substorm and magnetosphere characteristic scales inferred from the SuperMAG auroral electrojet indices.

*Journal of Geophysical Research (Space Physics)*, *116*(A12), A12232. doi: 10.1029/2011JA016936

Nishimura, Y., Bortnik, J., Li, W., Thorne, R. M., Chen, L., Lyons, L. R., ... Auster, U. (2011, November). Multievent study of the correlation between pulsating aurora and whistler mode chorus emissions. *Journal of Geophysical Research (Space Physics)*, *116*(A11), A11221. doi: 10.1029/2011JA016876

Nishimura, Y., Bortnik, J., Li, W., Thorne, R. M., Lyons, L. R., Angelopoulos, V., ... Auster, U. (2010, October). Identifying the Driver of Pulsating Aurora. *Science*, *330*(6000), 81. doi: 10.1126/science.1193186

Oguti, T., Kokubun, S., Hayashi, K., Tsuruda, K., Machida, S., Kitamura, T., ... Watanabe, T. (1981, August). Statistics of pulsating auroras on the basis of all-sky TV data from five stations. I. Occurrence frequency. *Canadian Journal of Physics*, *59*, 1150-1157. doi: 10.1139/p81-152

Ohtani, S., & Gjerloev, J. W. (2020, September). Is the Substorm Current Wedge an Ensemble of Wedgelets?: Revisit to Midlatitude Positive Bays. *Journal of Geophysical Research (Space Physics)*, *125*(9), e27902. doi: 10.1029/2020JA027902

Osepian, A., Kirkwood, S., Dalin, P., & Tereschenko, V. (2009, October). D-region electron density and effective recombination coefficients during twilight - experimental data and modelling during solar proton events. *Annales Geophysicae*, *27*(10), 3713-3724. doi: 10.5194/angeo-27-3713-2009

Oyama, S., Kero, A., Rodger, C. J., Clilverd, M. A., Miyoshi, Y., Partamies, N., ... Saito, S. (2017, June). Energetic electron precipitation and auroral morphology at the substorm recovery phase. *Journal of Geophysical Research (Space Physics)*, *122*(6), 6508-6527. doi: 10.1002/2016JA023484

Partamies, N., Whiter, D., Kadokura, A., Kauristie, K., Nesse Tyssøy, H., Massetti, S., ... Raita, T. (2017, May). Occurrence and average behavior of pulsating aurora. *Journal of Geophysical Research (Space Physics)*, *122*(5), 5606-5618. doi: 10.1002/2017JA024039

Royrvik, O., & Davis, T. N. (1977, October). Pulsating aurora: Local and global morphology. *Journal of Geophysical Research*, *82*(29), 4720. doi: 10.1029/JA082i029p04720

Sandahl, I., Eliasson, L., & Lundin, R. (1980, May). Rocket observations of precipitating electrons over a pulsating aurora. *Geophysical Research Letters*, *7*(5), 309-312. doi: 10.1029/GL007i005p00309

Semeter, J., & Kamalabadi, F. (2005, April). Determination of primary electron spectra from incoherent scatter radar measurements of the auroral E region. *Radio Science*, *40*(2), RS2006. doi: 10.1029/2004RS003042

Sivadas, N., Semeter, J., Nishimura, Y., & Kero, A. (2017, October). Simultaneous Measurements of Substorm-Related Electron Energization in the Ionosphere and the Plasma Sheet. *Journal of Geophysical Research (Space Physics)*, *122*(10), 10,528-10,547. doi: 10.1002/2017JA023995

Thorne, R. M., Smith, E. J., Fiske, K. J., & Church, S. R. (1974, January). Intensity variation of ELF hiss and chorus during isolated substorms. *Geophysical Research Letters*, *1*(5), 193-196. doi: 10.1029/GL001i005p00193

Tsurutani, B. T., & Smith, E. J. (1974, January). Postmidnight chorus: A substorm phenomenon. *Journal of Geophysical Research (Space Physics)*, *79*(1), 118-127. doi: 10.1029/JA079i001p00118

Tsurutani, B. T., & Smith, E. J. (1977, November). Two types of magnetospheric ELF chorus and their substorm dependences. *Journal of Geophysical Research*, *82*(32), 5112. doi: 10.1029/JA082i032p05112

Turunen, E., Kero, A., Verronen, P. T., Miyoshi, Y., Oyama, S.-I., & Saito, S. (2016, October). Mesospheric ozone destruction by high-energy electron precipitation associated with pulsating aurora. *Journal of Geophysical Research (Atmospheres)*, *121*(19), 11,852-11,861. doi: 10.1002/2016JD025015

Verronen, P. T., Kero, A., Partamies, N., Szelag, M. E., Oyama, S.-I., Miyoshi, Y., & Turunen, E. (2021, October). Simulated seasonal impact on middle atmospheric ozone from high-energy electron precipitation related to pulsating aurorae. *Annales Geophysicae*, *39*(5), 883-897. doi: 10.5194/angeo-39-883-2021

Vickrey, J. F., Vondrak, R. R., & Matthews, S. J. (1982, July). Energy deposition by precipitating particles and Joule dissipation in the auroral ionosphere. *Journal of Geophysical Research*, *87*(A7), 5184-5196. doi: 10.1029/JA087iA07p05184

Whalen, B. A., Miller, J. R., & McDiarmid, I. B. (1971, January). Energetic particle measurements in a pulsating aurora. *Journal of Geophysical Research*, *76*(4), 978. doi: 10.1029/JA076i004p00978

Wing, S., Gkioulidou, M., Johnson, J. R., Newell, P. T., & Wang, C.-P. (2013, March). Auroral particle precipitation characterized by the substorm cycle. *Journal of Geophysical Research (Space Physics)*, *118*(3), 1022-1039. doi: 10.1002/jgra.50160

| Date | Start Time (UTC) | End Time (UTC) |
|---|---|---|
| 2012-03-28 | 10:25:28 | 12:46:49 |
| 2012-12-20 | 11:12:07 | 16:18:47 |
| 2013-03-24 | 10:52:26 | 12:38:36 |
| 2014-11-02 | 12:40:31 | 13:31:41 |
| 2015-01-13 | 11:26:42 | 11:59:50 |
| 2015-01-14 | 10:32:55 | 10:54:12 |
| 2015-01-26 | 7:49:39 | 8:18:41 |
| 2015-02-26 | 9:46:46 | 10:45:44 |
| 2015-02-26 | 12:29:40 | 14:03:29 |
| 2015-03-12 | 10:01:48 | 10:44:22 |
| 2016-10-10 | 11:11:54 | 11:59:55 |
| 2016-10-13 | 12:49:20 | 13:59:51 |
| 2016-10-16 | 11:47:46 | 12:59:54 |
| 2016-10-19 | 10:33:39 | 12:15:24 |
| 2016-11-02 | 12:10:36 | 12:59:52 |
| 2016-11-13 | 9:24:40 | 10:59:49 |
| 2016-11-25 | 10:00:02 | 10:59:52 |
| 2016-12-11 | 9:51:00 | 9:59:56 |
| 2016-12-20 | 8:59:47 | 10:59:56 |
| 2016-12-26 | 10:32:15 | 10:59:51 |
| 2017-01-06 | 8:32:02 | 8:59:51 |
| 2017-03-30 | 12:10:59 | 13:04:47 |
| 2017-04-14 | 12:00:04 | 12:58:46 |
| 2017-04-18 | 12:00:01 | 12:31:27 |
| 2017-08-17 | 8:08:43 | 8:43:34 |
| 2017-09-03 | 9:36:22 | 10:45:19 |
| 2017-09-03 | 11:10:50 | 13:00:10 |
| 2017-09-14 | 11:30:31 | 14:00:05 |
| 2017-09-18 | 8:34:19 | 8:59:50 |
| 2018-10-23 | 11:05:32 | 11:35:47 |
| 2018-12-30 | 11:10:22 | 11:53:21 |
| 2019-01-06 | 12:00:07 | 12:59:53 |
| 2019-01-07 | 12:00:00 | 12:59:54 |
| 2019-01-26 | 13:47:03 | 13:59:48 |
| 2019-01-31 | 13:00:10 | 13:59:54 |
| 2019-02-01 | 13:00:09 | 13:59:49 |
| 2019-02-28 | 13:50:41 | 16:01:17 |
| 2019-03-01 | 10:04:47 | 12:04:41 |
| 2019-03-02 | 6:44:08 | 7:20:41 |
| 2019-03-28 | 13:45:12 | 14:06:12 |
| 2019-03-31 | 13:00:02 | 13:39:53 |
| 2019-04-03 | 13:00:11 | 13:48:53 |
| 2019-09-01 | 7:36:54 | 8:09:04 |
| 2019-09-01 | 9:14:12 | 10:21:35 |

| | | |
|---|---|---|
| 2019-09-01 | 11:39:50 | 13:15:49 |
| 2019-09-02 | 10:12:14 | 11:06:53 |
| 2019-09-03 | 12:28:43 | 13:19:55 |
| 2019-12-18 | 11:42:17 | 11:59:59 |
| 2019-12-19 | 8:23:32 | 9:46:10 |
| 2019-12-19 | 10:47:53 | 11:59:52 |
| 2020-01-04 | 11:36:36 | 12:47:11 |
| 2020-01-05 | 12:23:32 | 15:02:37 |
| 2020-01-31 | 11:51:52 | 13:22:28 |
| 2020-03-31 | 11:36:47 | 12:51:36 |
| 2020-03-31 | 13:00:22 | 13:54:27 |
| 2020-10-01 | 12:34:59 | 14:43:50 |
| 2021-01-13 | 11:08:54 | 14:26:32 |